Supplementary Information

for

Radiation Unlocks Selective and Efficient Gold Recovery

Corresponding author: Wei Cao, caowei@bnu.edu.cn

The PDF file includes:

Figs. S1 to S23
Tables S1 to S5
References

Table of Contents

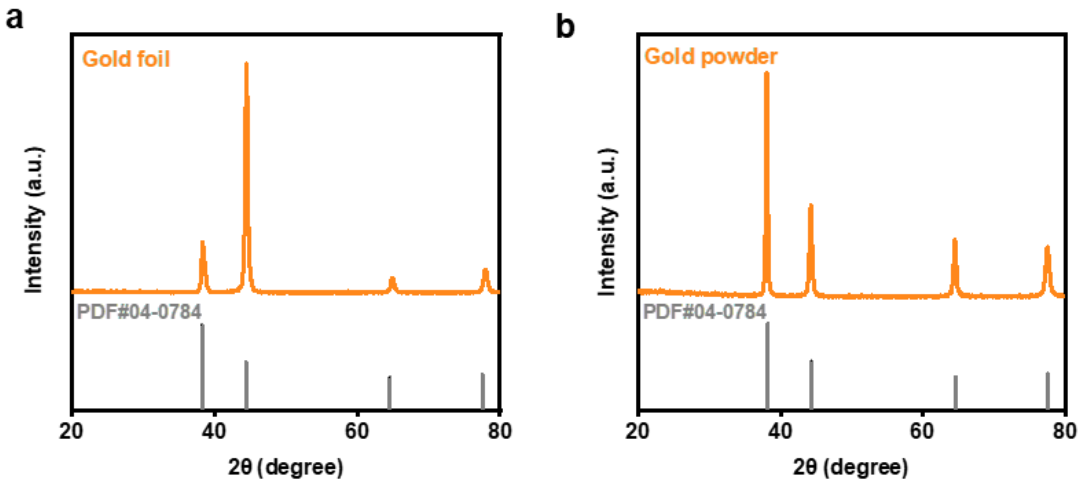

Fig. S1. XRD patterns of commercial gold materials. (a) Gold foil and (b) gold powder, both purchased from Nanjing Yong Foil Metal Materials Co., Ltd.

The intense diffraction peaks in both patterns are observed at 2θ values of approximately 38.2°, 44.4°, 64.6° and 77.5° which correspond to the (111), (200), (220) and (311) lattice planes of face-centered cubic (fcc) gold, respectively. All peak positions are in excellent agreement with the standard reference pattern for metallic gold (PDF#04-0784), confirming the high phase purity and crystalline nature of the purchased materials.

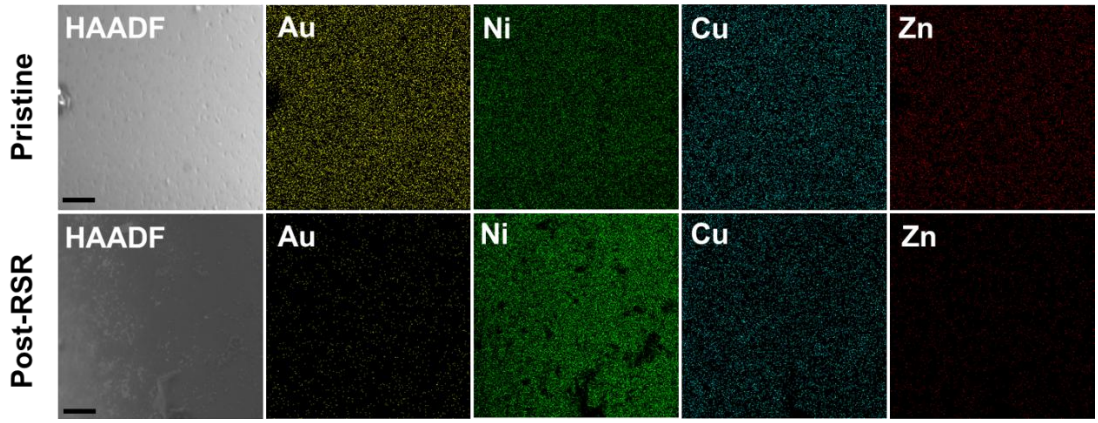

Fig. S2. SEM coupled with EDS shows the metal distribution on the surface of the side view of CPU pin before and after RSR (Scale bar=20 µm).

Gold (Au) is predominantly concentrated on the outer surface layer, while Ni, Cu and Zn signals are distributed within the underlying substrate. A remarkable decrease in the Au signal intensity is observed on the surface, while the signals of Ni, Cu, and Zn show no significant attenuation. Notably, the relative intensity of the Ni signal appears enhanced compared to the other non-precious metals after the selective removal of the surface Au layer.

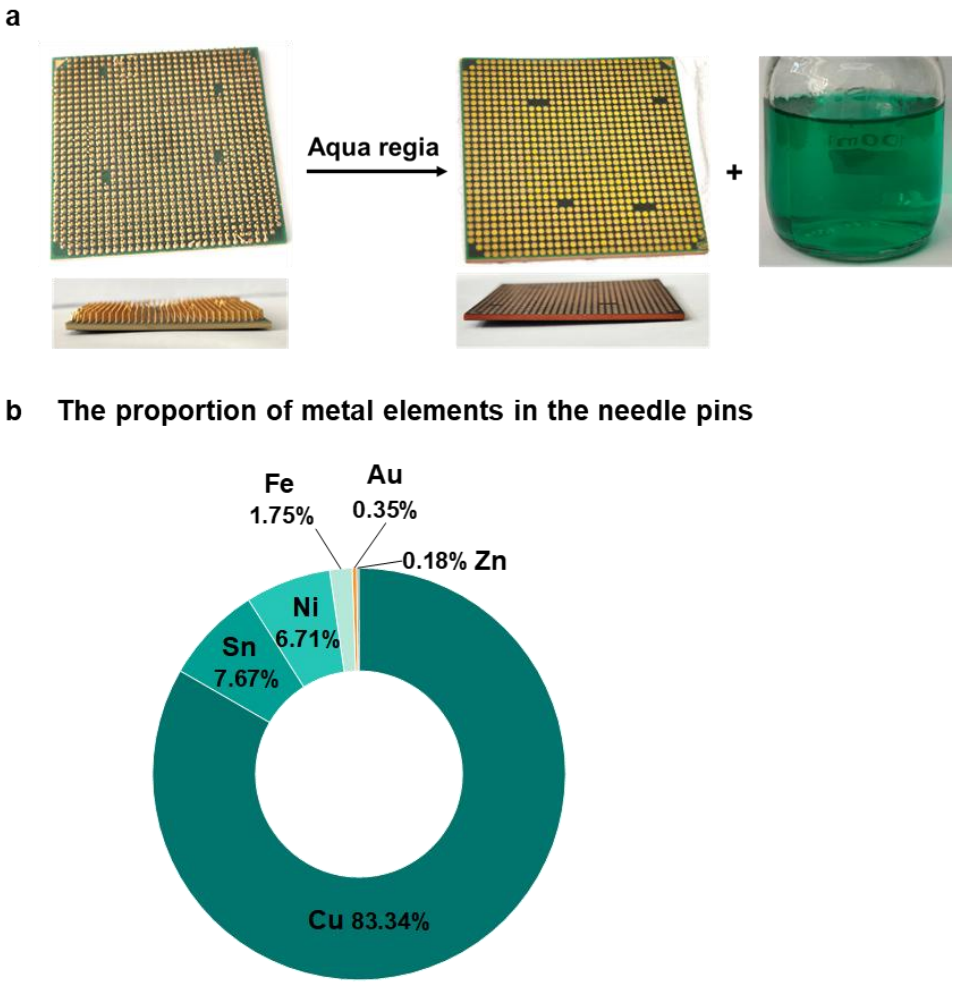

Fig. S3. (a) Photographs of CPU pin dissolution in aqua regia. (b) Elemental composition distribution in CPU pins.

Upon treatment with aqua regia, the metallic pins on the CPU board were completely dissolved, yielding a green solution. Bulk elemental composition of CPU pins as determined by ICP-OES analysis of the aqua regia digestate. The quantitative results are: copper (Cu, 83.34 wt%), tin (Sn, 7.67 wt%), nickel (Ni, 6.71 wt%), iron (Fe, 1.75 wt%), gold (Au, 0.35 wt%), zinc (Zn, 0.18 wt%).

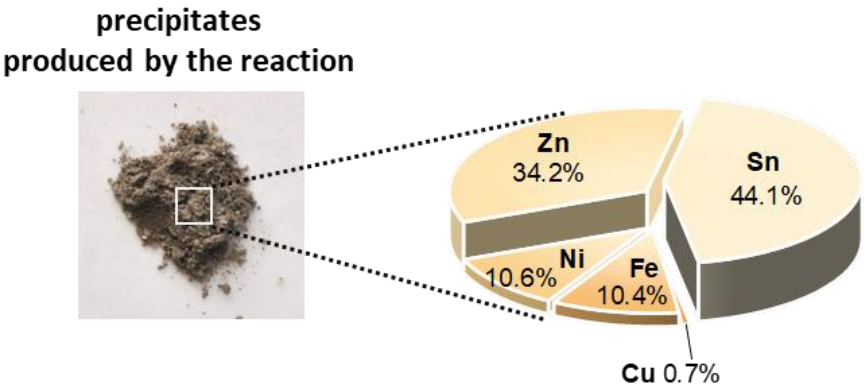

Fig. S4. Photo of the precipitates produced by RSR of end-of-life CPUs and the proportion of different metal elements in the precipitates.

Quantitative mass composition of the precipitate determined by ICP-OES: tin (Sn, 44.1 wt%), zinc (Zn, 34.2 wt%), nickel (Ni, 10.6 wt%), iron (Fe, 10.4 wt%), and copper (Cu, 0.7 wt%).

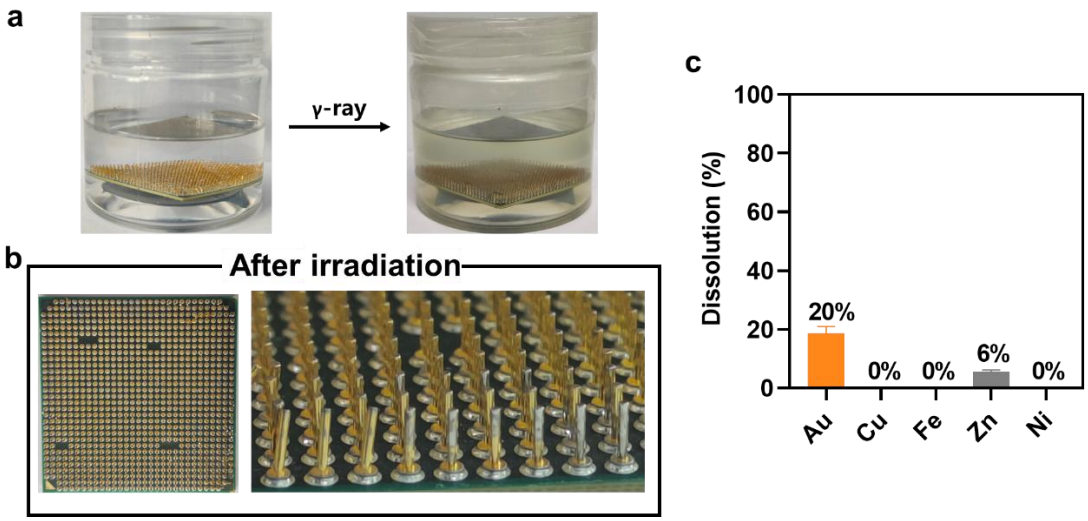

Fig. S5. RSR of Au from end-of-life CPU and its characterization.

(a) Photographs of CPU before and after RSR in 75% MeCN solution ($c(OH^-) = 10^{-9}$ M). (b) Post-irradiation detailed photographs of CPU and pins. (c) Dissolution percentages of various metals in CPU after irradiation. (The dissolution percentage obtained by the aqua regia method was set as 100%)

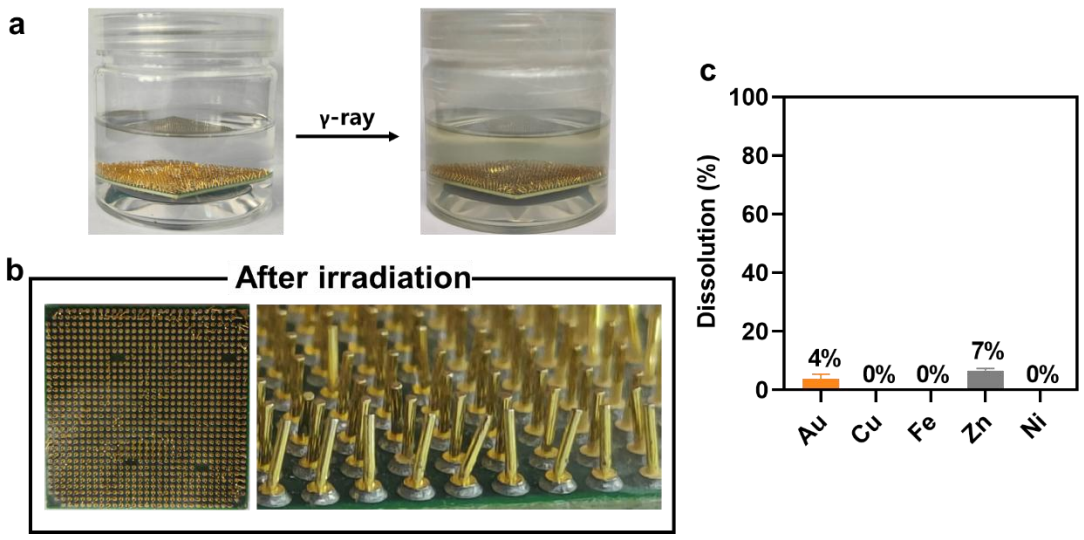

Fig. S6. RSR of Au from end-of-life CPU and its characterization.

(a) Photographs of CPU before and after RSR in 75% MeCN solution. ($c(OH^-) = 10^{-7}$ M) (b) Post-irradiation detailed photographs of CPU and pins. (c) Dissolution percentages of various metals in CPU after irradiation. (The dissolution percentage obtained by the aqua regia method was set as 100%)

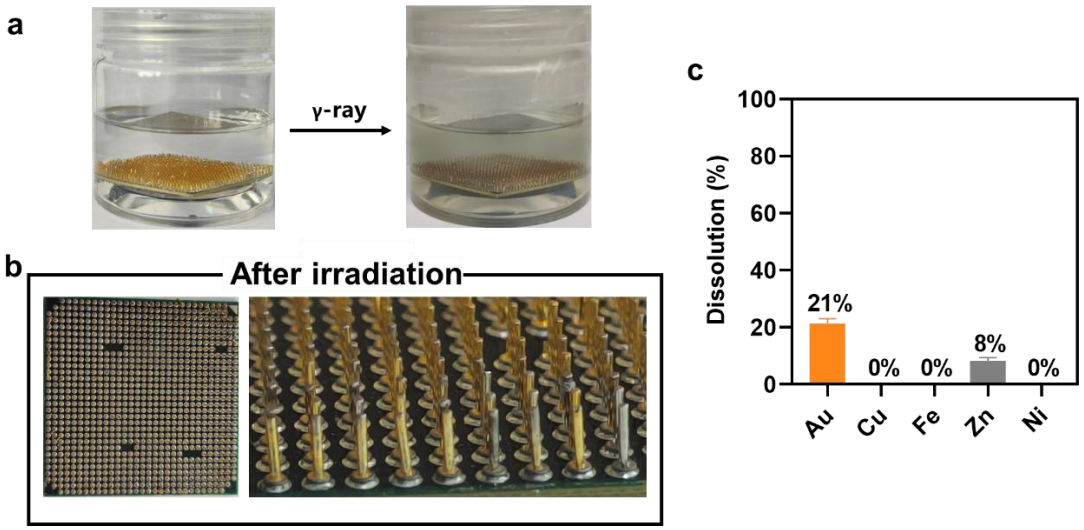

Fig. S7. RSR of Au from end-of-life CPU and its characterization.

(a) Photographs of CPU before and after RSR in 75% MeCN solution ($c(OH^-) = 10^{-6}$ M). (b) Post-irradiation detailed photographs of CPU and pins. (c) Dissolution percentages of various metals in CPU after irradiation. (The dissolution percentage obtained by the aqua regia method was set as 100%)

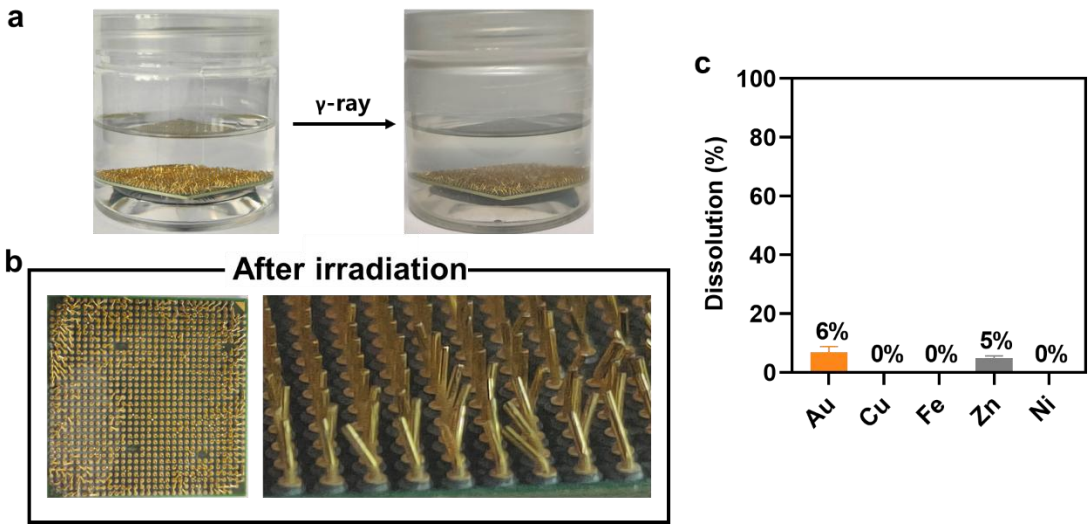

Fig. S8. RSR of Au from end-of-life CPU and its characterization.

(a) Photographs of CPU before and after RSR in 75% MeCN solution ($c(OH^-)=10^{-4}$ M). (b) Post-irradiation detailed photographs of CPU and pins. (c) Dissolution percentages of various metals in CPU after irradiation. (The dissolution percentage obtained by the aqua regia method was set as 100%)

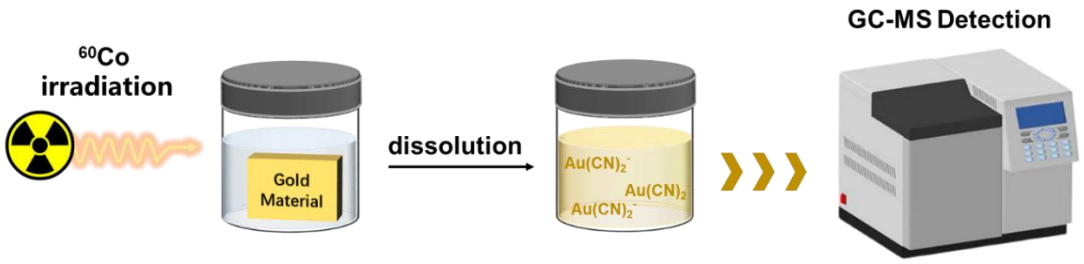

Fig. S9. Schematic diagram of GC-MS analysis for post-irradiation solution.

The analysis was performed on the filtrate obtained after immersing 2 mg of gold powder in acetonitrile aqueous solution, irradiating with a ^{60}Co source for 24 h, and subsequent membrane filtration.

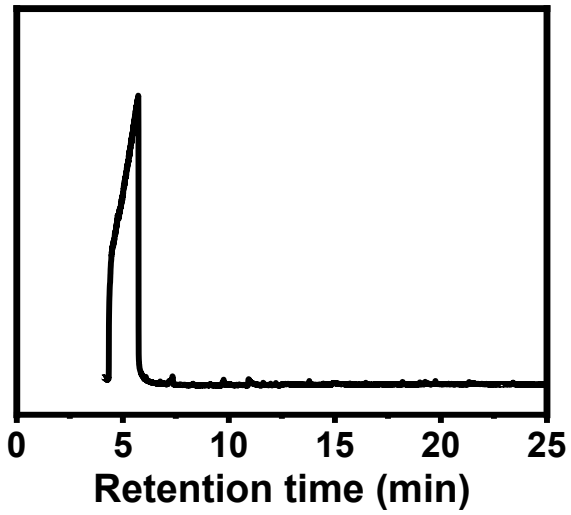

Fig. S10. Gas chromatography-mass spectrometry (GC-MS) chromatogram of the reaction solution.

Analysis conditions: injection volume, 1 μL; carrier gas flow rate, 1.0 mL/min; ion source temperature, 230 °C. The chromatogram reveals a distinct major peak at a retention time of approximately 5 min.

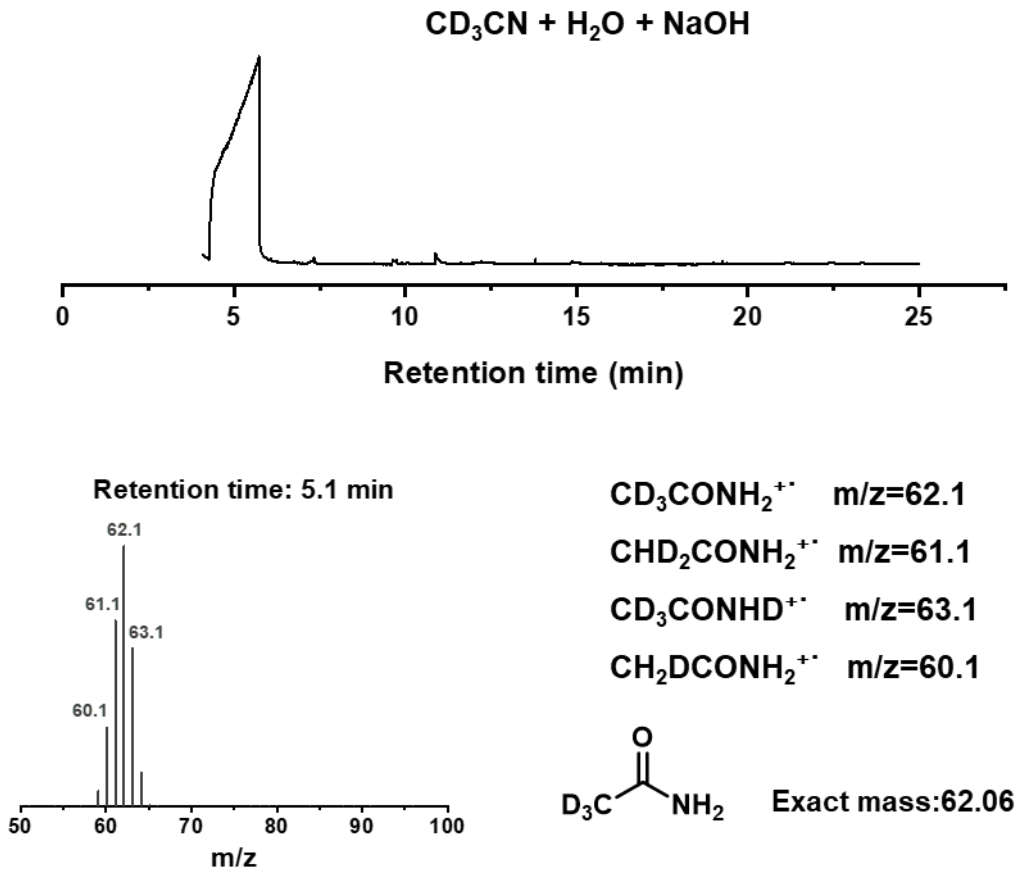

Fig. S11. GC-MS chromatogram of the liquid after irradiation in the CD_3CN-H_2O-NaOH solution system.

Analysis conditions: injection volume, 1 μL; carrier gas flow rate, 1.0 mL/min; ion source temperature, 230 °C. The chromatogram shows a distinct major peak at a retention time of ~5.1 min. The mass spectrum of this peak exhibit characteristic ions at m/z 60.1, 61.1, 62.1 and 63.1 (corresponding to the values marked in the figure), and the product molecular formulas corresponding to these peaks are as shown. This confirms the formation of acetamide.

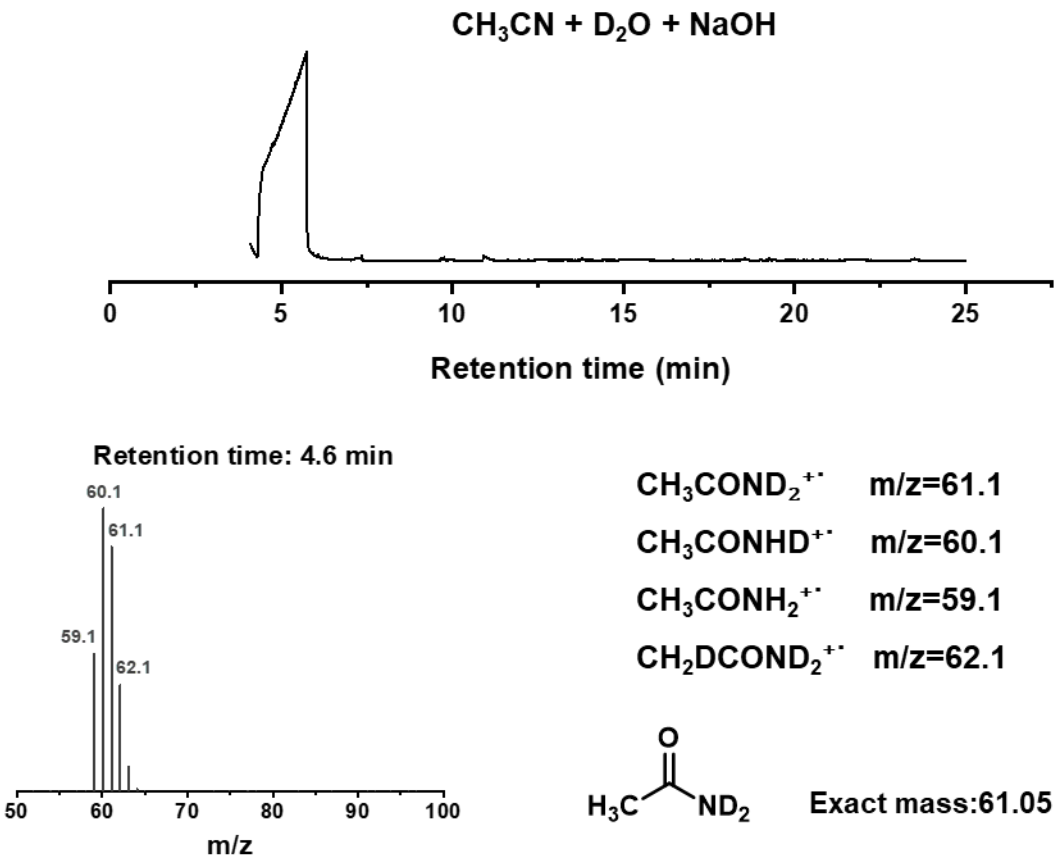

Fig. S12. GC-MS chromatogram of the liquid after irradiation in the CH_3CN-D_2O-NaOH solution system.

Analysis conditions: injection volume, 1 μL; carrier gas flow rate, 1.0 mL/min; ion source temperature, 230 °C. The chromatogram shows a distinct major peak at a retention time of ~4.6 min. The mass spectrum of this peak exhibit characteristic ions at m/z 59.1, 60.1, 61.1 and 62.1 (corresponding to the values marked in the figure), and the product molecular formulas corresponding to these peaks are as shown. This confirms the formation of acetamide.

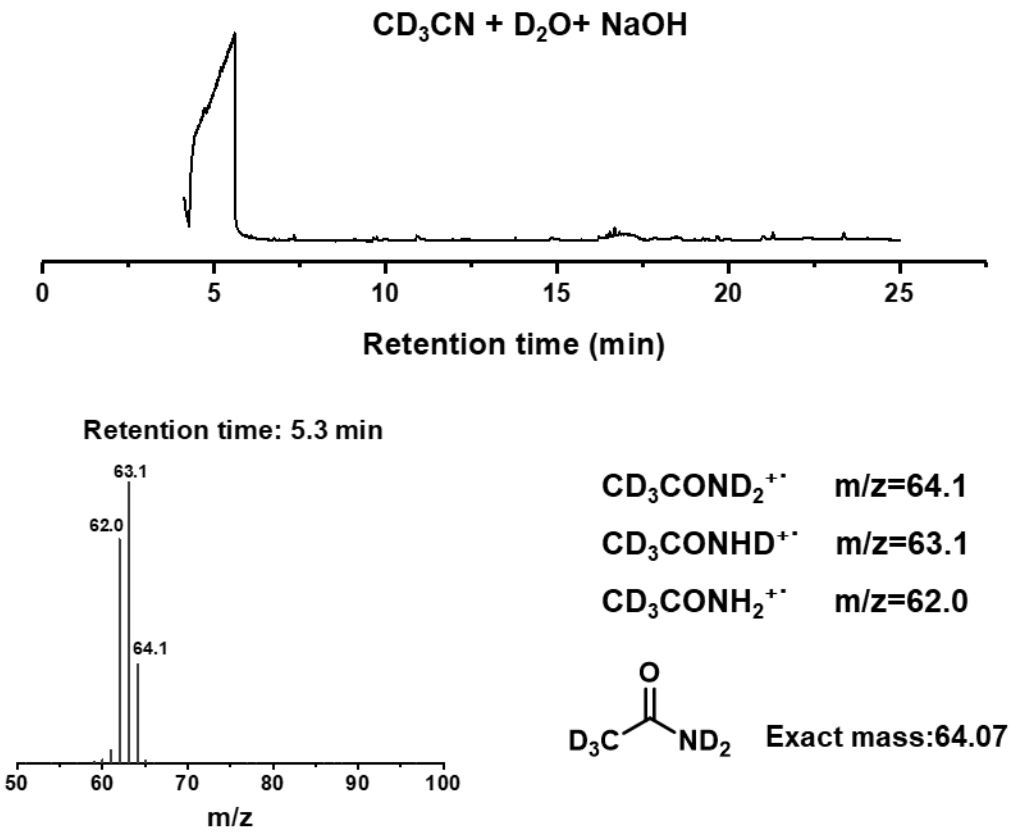

Fig. S13. GC-MS chromatogram of the liquid after irradiation in the CD_3CN-D_2O-NaOH solution system.

Analysis conditions: injection volume, 1 μL; carrier gas flow rate, 1.0 mL/min; ion source temperature, 230 °C. The chromatogram shows a distinct major peak at a retention time of ~5.3 min. The mass spectrum of this peak exhibit characteristic ions at m/z 62.0, 63.1 and 64.1 (corresponding to the values marked in the figure), and the product molecular formulas corresponding to these peaks are as shown. This confirms the formation of acetamide.

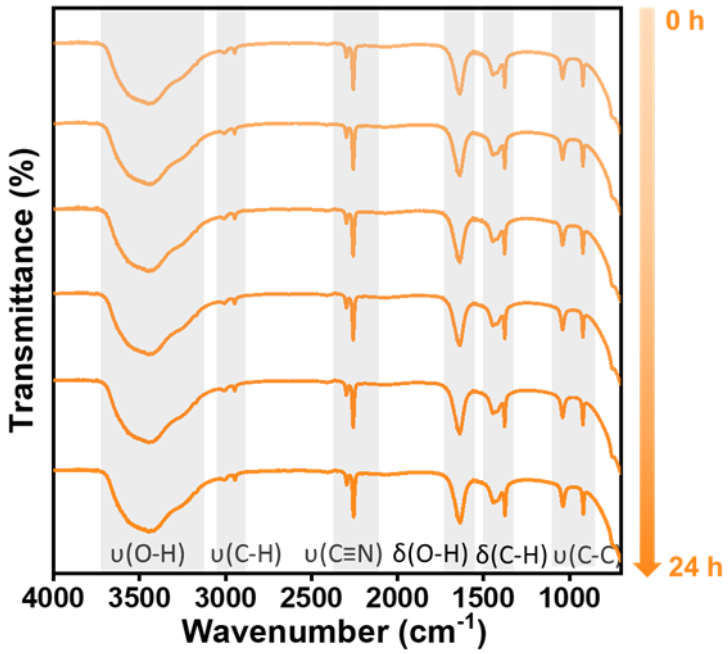

Fig. S14. Fourier-transform infrared spectra of the RSR reaction solution at different irradiation time.

The broad peak near 3500 cm^{-1} is assigned to the O–H stretching vibration (ν(O–H)). The peak near 2900 cm^{-1} is assigned to the C–H stretching vibration (ν(C–H)). The peak near 2250 cm^{-1} is assigned to the nitrile group stretching vibration (ν(C≡N)). The peak near 1600 cm^{-1} is assigned to the bending vibration of the O–H bond of water (δ(O-H)). The peak near 1400 cm^{-1} is assigned to the C–H bending vibration (δ(C-H)). The peak near 1000 cm^{-1} is assigned to the C–C stretching vibration (ν(C-C)). The intensity of the infrared absorption bands showed no significant change with increasing irradiation time. To highlight the spectral changes induced by the reaction, the unirradiated solution was used as the background for IR measurement. The resulting differential spectrum (Fig. 4F) revealed that with prolonged irradiation, the intensity of the broad band around 3400 cm^{-1} (corresponding to N–H stretching vibrations) increased. Concurrently, a growing absorption band emerged around 1600 cm^{-1}, which is characteristic of the C=O stretching vibration. These spectral changes collectively confirm the formation of acetamide during the irradiation process.

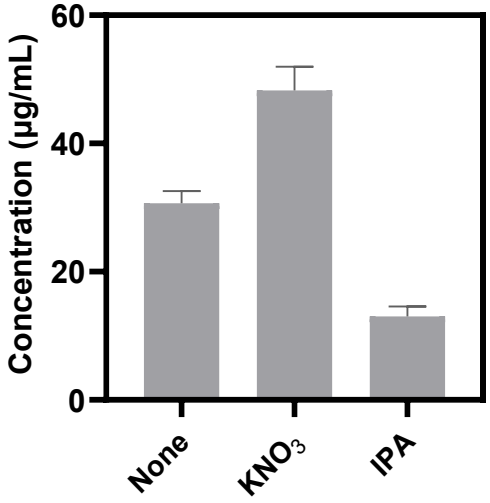

Fig. S15. Gold ion concentration following gold dissolution in the presence of various free radical scavengers.

For the hydrated electron quenching experiment, 2 mg gold powder was dispersed in 20 mL acetonitrile aqueous solution. Then, 1 mL of a 0.4 M KNO_3 solution was added. The mixture was then irradiated in a ^{60}Co source for 3 h. For the hydroxy radical quenching experiment, 2 mg gold powder was dispersed in 20 mL acetonitrile aqueous solution. Then, 1 mL of tert-butanol was added. The mixture was then irradiated in a ^{60}Co source for 3 h.

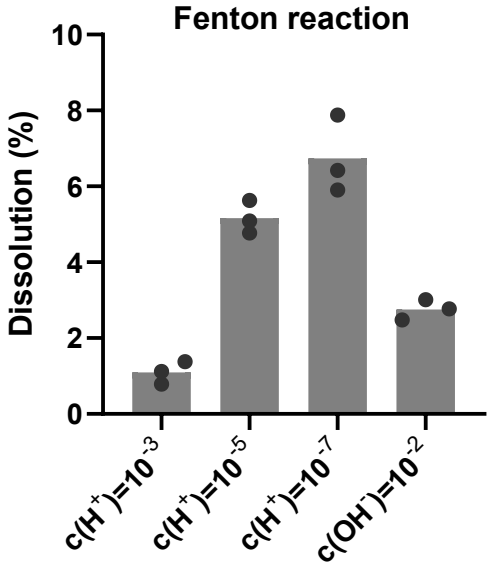

Fig. S16. Dissolution percentages of gold powder in Fenton/acetonitrile systems. (Experimental conditions: 75% acetonitrile aqueous solution, $c(H^+) = 10^{-3}/10^{-5}/10^{-7}$ M, $c(OH^-) = 10^{-2}$ M, 27.8 mg iron (II) sulfate and 120 μL 30% H_2O_2)

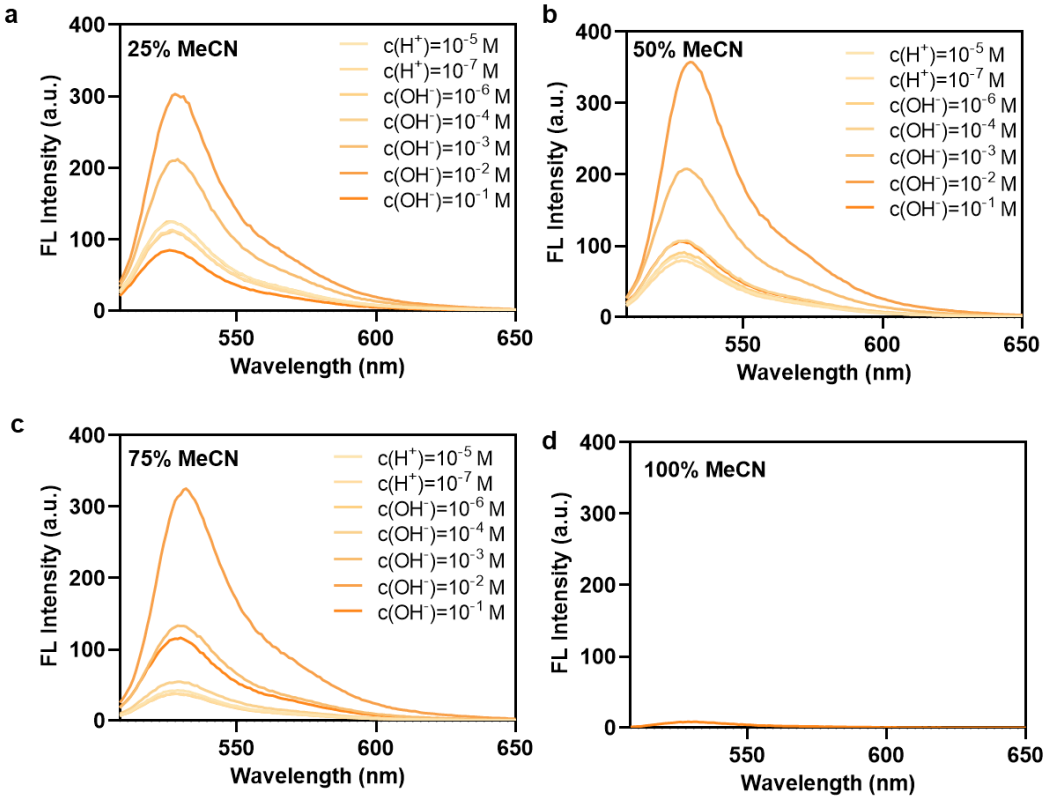

Fig. S17. Fluorescence spectra of Dichlorofluorescein (DCF). DCF was generated from Dichlorofluorescein diacetate (DCFH-DA) under irradiation in (a) 25%, (b) 50%, (c) 75%, (d) 100% acetonitrile aqueous solutions with varying acid/base concentrations. The excitation wavelength was set at 350 nm, with both the excitation and emission slits at 5 nm.

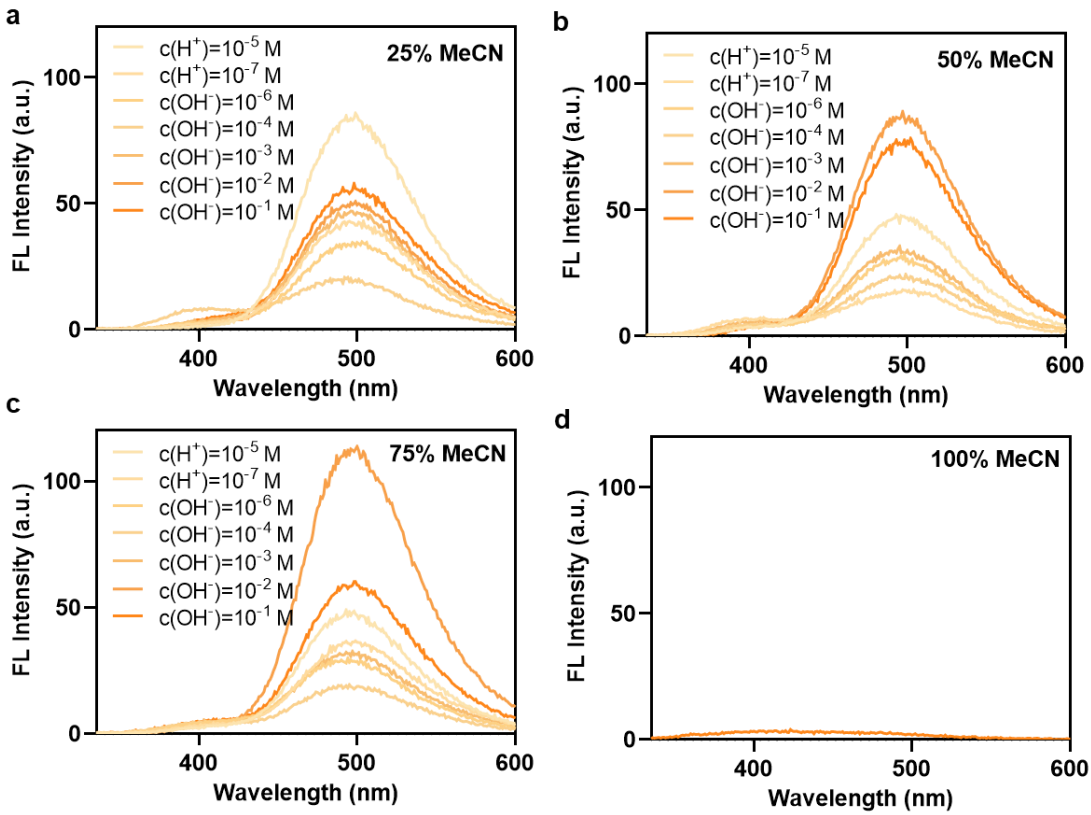

Fig. S18. Fluorescence spectra of 7-hydroxycoumarin. 7-hydroxycoumarin was generated from coumarin under irradiation in (a) 25%, (b) 50%, (c) 75%, (d) 100% acetonitrile aqueous solutions with varying acid/base concentrations. The excitation wavelength was set at 350 nm, with both the excitation and emission slits at 5 nm.

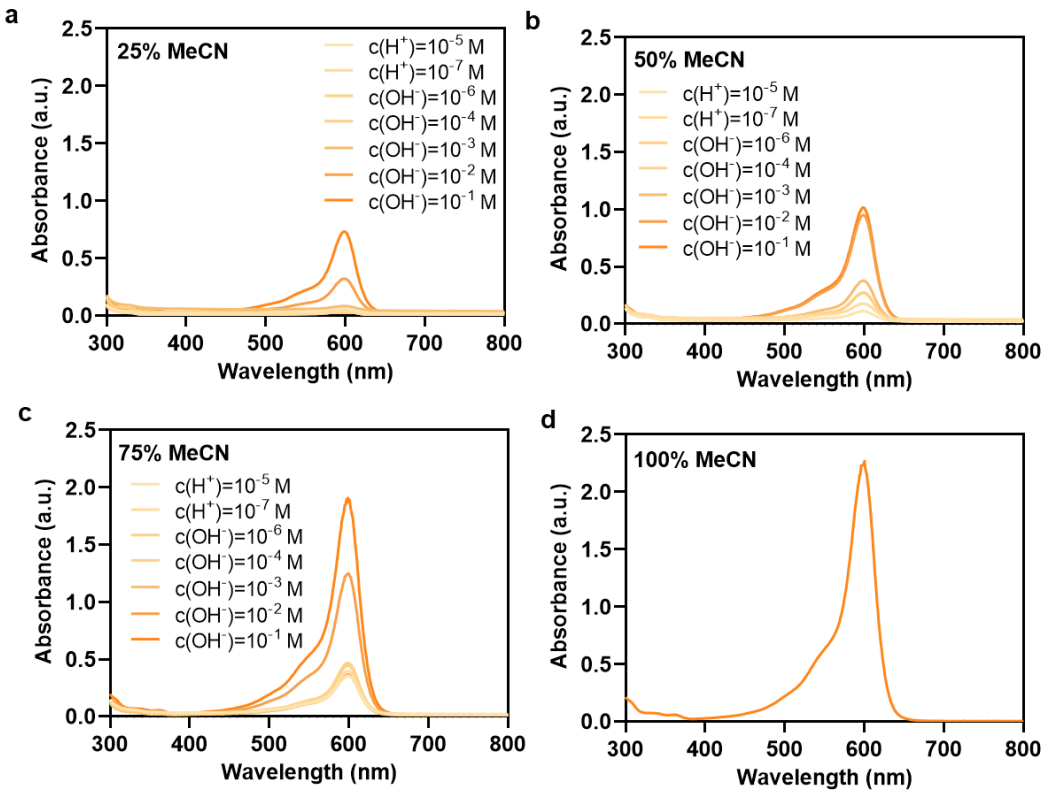

Fig. S19. UV-Vis absorption spectra of the blue-purple product. Blue-purple product was generated from the reaction of cyanide ions with isonicotinic acid-barbituric acid in irradiated CH_3CN solutions ((a) 25%, (b) 50%, (c) 75%, (d) 100%) with different acid/base concentrations. The slit width was set to 2 nm.

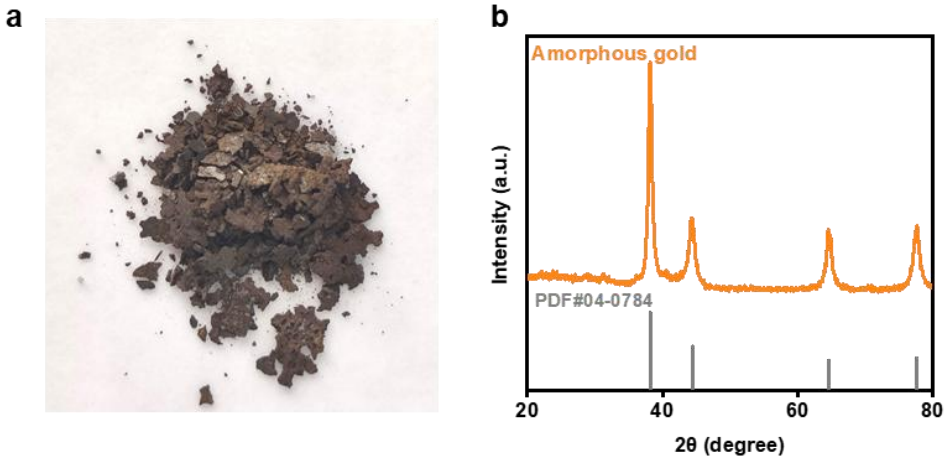

Fig. S20. (a) Photo of amorphous gold obtained from large-scale RSR experiments. (b) X-ray diffraction (XRD) pattern of amorphous gold.

The pattern exhibits broad diffraction features. The positions of the maxima in these broad features are centered at approximately 2θ = 38.2°, 44.4°, 64.6° and 77.5°, which correspond to the (111), (200), (220) and (311) lattice planes of face-centered cubic (fcc) gold, respectively. These peak positions are consistent with the reference data for metallic gold (PDF#04-0784), confirming its chemical identity.

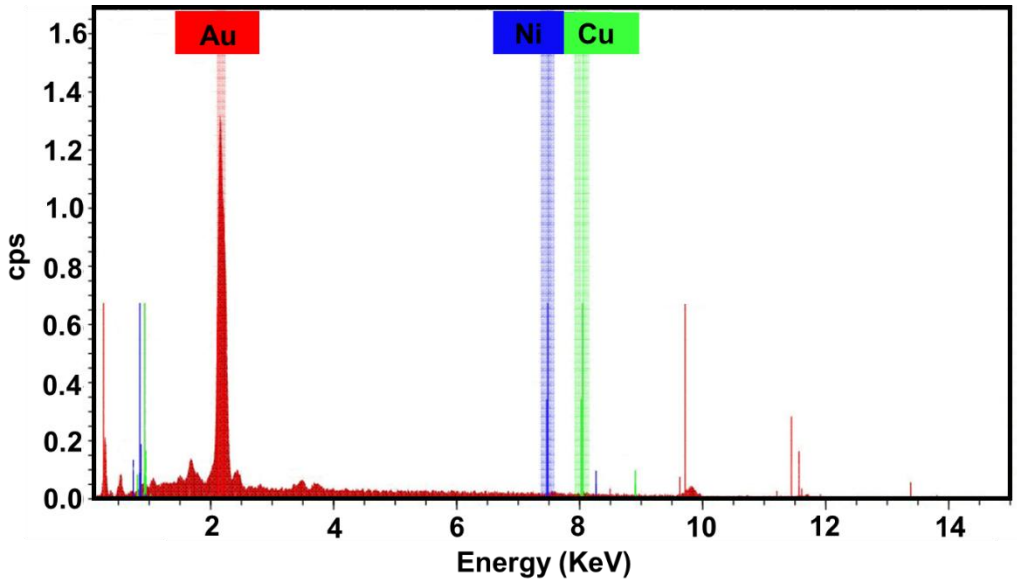

Fig. S21. Energy-dispersive X-ray spectroscopy (EDS) spectrum of gold obtained from the large-scale recovery.

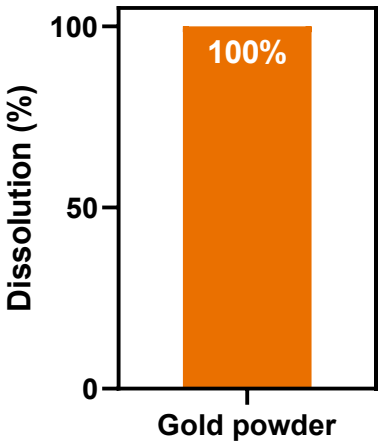

Fig. S22. Dissolution percentage of gold powder irradiated for 2 min under electron-beam.

Gold powder was irradiated for 2 min using an electron beam (dose rate: 330 Gy/min) in a solvent of c(NaOH) = 10^{-2} M with 75% MeCN. Under these optimized conditions, complete (100%) dissolution of gold was achieved.

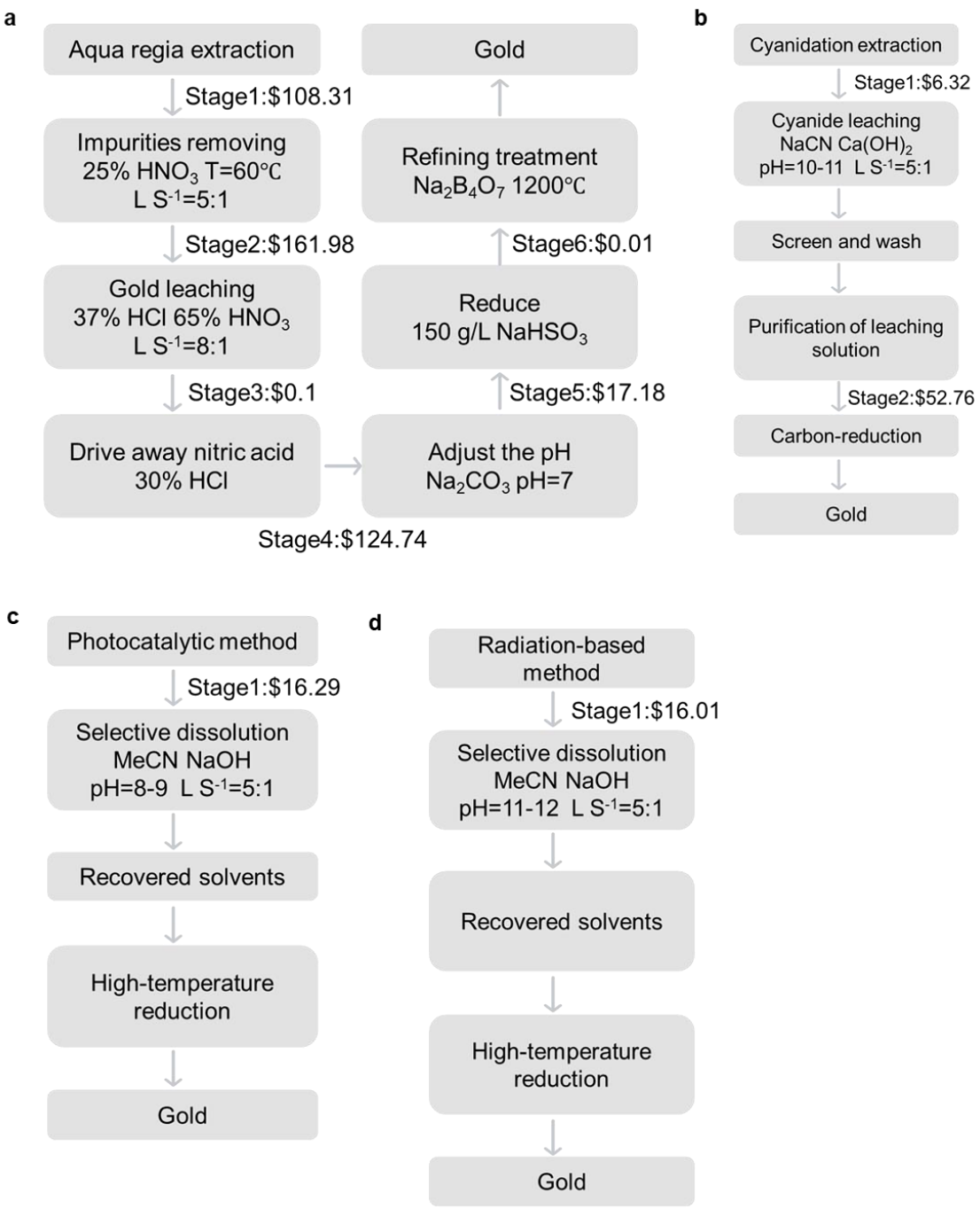

Fig. S23. Flowcharts for gold recovery processes.

(a) Process for gold extraction via aqua regia leaching; (b) Process for gold extraction via cyanidation; (c) Process for gold extraction via photocatalytic; (d) Process for gold extraction via Radiation-mediated Selective Recovery[1,2]. (adapted from *ACS Sustain. Chem. Eng*. 2019, 7, 7260–7267; *Nat. Chem. Eng.* 2024, 1, 170–179)

Table S1. Diameter and corresponding concentration of gold nanoparticles

	Gold nanoparticles
Diameter	16 nm
Concentration	2.39 nM

$$\lambda_{max} = 522\ nm, A_{522\ nm} \approx 1.057, A_{450\ nm} \approx 0.636$$

$$\frac{A_{522\ nm}}{A_{450\ nm}} = \frac{1.057}{0.636} \approx 1.66$$

According to the tabulated data relating gold nanoparticle diameters to their absorbance ratios[3].

$$d = 16\ nm, \varepsilon_{450\ nm} = 2.67 \times 10^{8}\ M^{-1}cm^{-1}$$

$$c_{NP} = \frac{A_{450\ nm}}{\varepsilon_{450\ nm}} = 2.39 \times 10^{-9}\ M = 2.39\ nM$$

$$m_{single\ NP} = V_{NP} \times \rho_{Au} = \frac{4}{3}\pi r^3 \times \rho_{Au} = \frac{4}{3}\pi \times (8\ \times\ 10^{-7}cm)^3 \times 19.32\ g/cm^3 \approx 4.14\ \times\ 10^{-17}\ g$$

$$M_{NP} = m_{single\ NP} \times N_A = 4.14\ \times\ 10^{-17}g \times 6.022\ \times\ 10^{23}mol^{-1} \approx 2.5\ \times\ 10^{7}\ g/mol$$

$$c_{Au} = c_{NP} \times M_{NP} = 2.39\ nM \times 2.5\ \times 10^{7} g/mol \approx 60\ mg/L$$

Table S2. Gold ion concentration and kinetic isotope effect (KIE) values in different solvent systems.

(Solvent: CH_3CN/H_2O, CH_3CN/D_2O, CD_3CN/H_2O, and CD_3CN/D_2O. Irradiated with ^{60}Co source for 2 h.)

	Au^+ Concentration (μg/mL)
H_2O+CH_3CN	95.44
H_2O+CD_3CN	89.00
D_2O+CH_3CN	94.70
D_2O+CD_3CN	82.84

$$KIE(water) = \frac{[Au]_{(H_2O+CH_3CN)}}{[Au]_{(D_2O+CD_3CN)}} = 1.008$$

$$KIE(ACN) = \frac{[Au]_{(H_2O+CH_3CN)}}{[Au]_{(H_2O+CD_3CN)}} = 1.072$$

$$KIE(total) = \frac{[Au]_{(H_2O+CH_3CN)}}{[Au]_{(D_2O+CD_3CN)}} = 1.152$$

Table S3. G-values of various substances during ionizing radiation[4]

Compound	G-value	nM/Gy
·OH	2.7	280
Au^{+}	0.5	51

In radiation chemistry, G-value is defined as the number of events per 100 eV of absorbed energy[5].

$$G(nM/Gy) = \frac{c(Au^{+})}{radiation\ dose(Gy)} = \frac{5.1 \times 10^{-4}\ M}{1 \times 10^{4}\ Gy} \times 10^{9} = 51\ nM/Gy$$

$$1\ G = 1.0364 \times 10^{-7}\ mol \cdot J^{-1}$$

$$G = \frac{G(nM/Gy) \times 10^{-9}}{1.0364 \times 10^{-7}} = \frac{5.1 \times 10^{1} \times 10^{-9}}{1.0364 \times 10^{-7}} = 0.5$$

Table S4. Ksp of various metal hydroxide and the pH at which non-precious metal ions begin to precipitate as hydroxides[1]

Non-precious metal ions	Hydroxide	K_{sp}^{θ}	pH
Zn^{2+}	$Zn(OH)_2$	3×10^{-17}	8.2
Sn^{2+}	$Sn(OH)_2$	5.45×10^{-28}	2.9
Fe^{2+}	$Fe(OH)_2$	4.87×10^{-17}	8.3
Fe^{3+}	$Fe(OH)_3$	4.0×10^{-38}	3.5
Ni^{2+}	$Ni(OH)_2$	5.48×10^{-16}	8.9
Cu^{2+}	$Cu(OH)_2$	2.2×10^{-20}	6.7

Table S5. Materials costs of aqua regia, cyanidation, photocatalytic selective dissolution and radiation-mediated dissolution[1]. (Recovery of 1 kg CPU)

The cost data for aqua regia extraction, cyanidation extraction and photocatalytic selective dissolution are referenced from *Nat. Chem. Eng.* 2024, 1, 170 – 179, while the costs for radiation-mediated dissolution are estimated based on the consumption of reagents in this work. The price parameters for these reagents are adopted from *Nat. Chem. Eng.* 2024, 1, 170 – 179.

Method	Material	Source	Cost	Minimum Cost	Total Cost
Aqua regia extraction	Hydrochloric acid (HCl, 37%)	Titan Co. Aladdin Reagent Co. Sinopharm Chemical Reagent Co.	\$108.47/L \$28.87/L \$6.94/L	\$6.94/L	\$412.32
	Nitric acid (HNO_3, 69%)	Adama Reagent Co. Aladdin Reagent Co. Alfa Esha Chemical Co	\$209.45/L \$60.17/L \$445.47/L	\$60.17/L	
	Sodium Carbonate (Na_2CO_3)	Aladdin Reagent Co. Fisher Chemical Co. Acros Co.	\$98.07/kg \$51.98/kg \$91.35/kg	\$51.98/kg	
	Sodium Hydrogen Sulfite ($NaHSO_3$)	Acros Co. Macklin Biochemical Technology Co.	\$176.82/kg \$14.32kg	\$14.32/kg	
	Sodium tetraborate ($Na_2B_4O_7$)	Acros Co. Aladdin Reagent Co. Fisher Co.	\$56.46/kg \$62.06/kg \$55.62/kg	\$55.62/kg	
Cyanidation	Sodium cyanide (NaCN)	Hubei Xinrunde Chemical Co.	\$2.54/kg	\$2.54/kg	\$59.08

extraction	Calcium hydroxide ($Ca(OH)_2$)	Aladdin Reagent Co. Alfa Esha Chemical Co. Macklin Biochemical Technology Co.	$105.51/kg $258.72/kg $109.85/kg	$105.51/kg	
	Active carbon (C)	Lok Yan Co. Sheen's Co.	$65.57/kg $16.39/kg	$16.39/kg	
Photocatalytic selective dissolution	Acetonitrile (CH_3CN, ≥99.0%)	Innochem Co. Aladdin Reagent Co. Alfa Co.	$5.4/L $41.89/L $59.26/L	$5.4/L	$16.29
	Sodium hydroxide (NaOH, 96%)	Macklin Biochemical Technology Co.	$11.85/kg	$11.85/kg	
	TiO_2 (P25)	Innochem Co. Acros Co.	$70.05/kg $60.38/kg	$60.38/kg	
This work: Radiation-mediated selective dissolution	Acetonitrile (CH_3CN, ≥99.0%)	Innochem Co. Aladdin Reagent Co. Alfa Co.	$5.4L $41.89/L $59.26/L	$5.4/L	$16.01
	Sodium hydroxide (NaOH, 96%)	Macklin Biochemical Technology Co.	$11.85/kg	$11.85/kg	

Reference

1. Shang, H. *et al.* Scalable and selective gold recovery from end-of-life electronics. *Nat. Chem. Eng.* **1**, 170–179 (2024).
2. Wang, J., Lu, Y. & Xu, Z. Identifying Extraction Technology of Gold from Solid Waste in Terms of Environmental Friendliness. *ACS Sustain. Chem. Eng.* **7**, 7260–7267 (2019).
3. Haiss, W., Thanh, N. T. K., Aveyard, J. & Fernig, D. G. Determination of Size and Concentration of Gold Nanoparticles from UV−Vis Spectra. *Anal. Chem.* **79**, 4215–4221 (2007).
4. Fu, Q. *et al.* Bioorthogonal chemistry for prodrug activation *in vivo*. *Chem. Soc. Rev.* **52**, 7737–7772 (2023).
5. Butarbutar, S. L., Sanguanmith, S., Meesungnoen, J., Sunaryo, G. R. & Jay-Gerin, J.-P. Calculation of the Yields for the Primary Species Formed from the Radiolysis of Liquid Water by Fast Neutrons at Temperatures between 25–350°C. *Radiat. Res.* **181**, 659–665 (2014).